

Explainable Depression Classification Based on EEG Feature Selection From Audio Stimuli

Lixian Zhu[®], Rui Wang[®], Xiaokun Jin[®], Yuwen Li, Fuze Tian[®], Ran Cai[®], Kun Qian[®], *Senior Member, IEEE*, Xiping Hu[®], Bin Hu[®], *Fellow, IEEE*, Yoshiharu Yamamoto[®], *Member, IEEE*, and Björn W. Schuller[®], *Fellow, IEEE*

Abstract—With the development of affective computing and Artificial Intelligence (AI) technologies, Electroencephalogram (EEG)-based depression detection methods have been widely proposed. However, existing studies have mostly focused on the accuracy of depression recognition, ignoring the association between features and models.

Received 4 March 2024; revised 23 December 2024 and 11 March 2025; accepted 29 March 2025. Date of publication 2 April 2025; date of current version 21 April 2025. This work was supported in part by the National Natural Science Foundation of China under Grant 62227807, Grant 62402041, Grant 12374171, Grant 62072219, Grant 61802159, and Grant 62272044; in part by the Ministry of Science and Technology of the People's Republic of China with the STI2030-Major Projects under Grant 2021ZD0201900, Grant 2021ZD0200408, and Grant 2021ZD0200601; in part by the National Key Research and Development Program of China under Grant 2023YFC2506804, Grant 2019YFA0706200, and Grant 2022YFC3500503; and in part by the Fundamental Research Funds for the Central Universities. (Lixian Zhu and Rui Wang contributed equally to this work.) (Corresponding authors: Fuze Tian; Kun Qian; Bin Hu.)

This work involved human subjects or animals in its research. Approval of all ethical and experimental procedures and protocols was granted by the local Ethics Committee for Biomedical Research at Lanzhou University Second Hospital, under Approval No. 2022A-620.

Lixian Źhu, Rui Wang, Xiaokun Jin, Yuwen Li, Ran Cai, Kun Qian, and Xiping Hu are with the Key Laboratory of Brain Health Intelligent Evaluation and Intervention, Ministry of Education, School of Medical Technology, Beijing Institute of Technology, Beijing 100081, China (e-mail: zhulx17@bit.edu.cn; wangr@bit.edu.cn; jinxk@bit.edu.cn; lyw_bit@bit.edu.cn; cairan20@bit.edu.cn; qian@bit.edu.cn; huxp@bit.edu.cn).

Fuze Tian is with the School of Information Science and Engineering, Lanzhou University, Lanzhou 730000, China (e-mail: tianfz17@lzu. edu.cn).

Bin Hu is with the Key Laboratory of Brain Health Intelligent Evaluation and Intervention, Ministry of Education, and the School of Medical Technology, Beijing Institute of Technology, Haidian, Beijing 100081, China, also with Gansu Provincial Key Laboratory of Wearable Computing, School of Information Science and Engineering, Lanzhou University, Lanzhou 730000, China, also with the CAS Center for Excelence in Brain Science and Intelligence Technology, Shanghai Institutes for Biological Sciences, Chinese Academy of Sciences, Shanghai 200234, China, and also with the Joint Research Center for Cognitive Neurosensor Technology of Lanzhou University and Institute of Semiconductors, Chinese Academy of Sciences, Lanzhou 730000, China (e-mail: bh@bit.edu.cn).

Yoshiharu Yamamoto is with the Educational Physiology Laboratory, Graduate School of Education, The University of Tokyo, Bunkyo, Tokyo 113-0033, Japan (e-mail: yamamoto@p.u-tokyo.ac.jp).

Björn W. Schuller is with GLAM—the Group on Language, Audio, and Music, Imperial College London, SW7 2AZ London, U.K., also with the Chair of Health Informatics (CHI), MRI, Technische Universität München, 81675 Munich, Germany, also with Munich Data Science Institute (MDSI), 85748 Munich, Germany, and also with Munich Center for Machine Learning (MCML), 80538 Munich, Germany (e-mail: schuller@ieee.org).

Digital Object Identifier 10.1109/TNSRE.2025.3557275

Additionally, there is a lack of research on the contribution of different features to depression recognition. To this end, this study introduces an innovative approach to depression detection using EEG data, integrating Ant-Lion Optimization (ALO) and Multi-Agent Reinforcement Learning (MARL) for feature fusion analysis. The inclusion of Explainable Artificial Intelligence (XAI) methods enhances the explainability of the model's features. The Time-Delay Embedded Hidden Markov Model (TDE-HMM) is employed to infer internal brain states during depression, triggered by audio stimulation. The ALO-MARL algorithm, combined with hyper-parameter optimization of the XGBoost classifier, achieves high accuracy (93.69%), sensitivity (88.60%), specificity (97.08%), and F1-score (91.82%) on a auditory stimulus-evoked three-channel EEG dataset. The results suggest that this approach outperforms state-of-the-art feature selection methods for depression recognition on this dataset, and XAI elucidates the critical impact of the minimum value of Power Spectral Density (PSD), Sample Entropy (SampEn), and Rényi Entropy (Ren) on depression recognition. The study also explores dynamic brain state transitions revealed by audio stimuli, providing insights for the clinical application of Al algorithms in depression recognition.

Index Terms— EEG, depression detection, ant lion optimization - multi-agent reinforcement learning (ALO-MARL), explainable artificial intelligence (XAI).

I. INTRODUCTION

EPRESSION has evolved into a comparatively prevalent mental health disorder with the progression of societal advancement [1]. The World Health Organization (WHO) predicts that depression will be the second leading cause of disability and death by 2030 [2], [3]. Besides, the outbreak and spread of COVID-19 have led to a rapid increase in the prevalence of depression in recent years. Mild depression patients may suffer from bad mood, lack of sleep, and mental malaise, while severe depression patients potentially even having suicidal behaviour [4]. Traditional diagnostic methods are standard scales evaluations – usually through subjective interviews, which are susceptible to environmental and individual differences. With the development of affective computing, the Electroencephalogram (EEG), as a non-invasive measure of electro-physiological signals with a millisecond time resolution, has been a potential tool to investigate the brain functions and cognitive processes in both healthy and diseased subjects, at rest [5], or during a task [6]. Several studies have demonstrated the relationship between depression and the EEG

signal obtained from prefrontal-lobe EEG sites, showing its validity as a physiological marker in depression [7], [8], [9], [10], [11], [12]. Furthermore, in the domain of EEG signal processing, the selection of EEG features emerges as a pivotal step, entailing the identification of paramount features for ensuing predictive analyses [13]. Efficacious feature selection is instrumental in diminishing dimensionality, augmenting prediction accuracy, and enhancing the intelligibility of results. However, the quest for the optimal feature subset within the expansive feature subset space presents a conventional challenge of considerable magnitude. Concurrently, existing methodologies exhibit a discernible deficiency in elucidating the correlation between models and features, thus leading to a lack of interpretability.

The existing body of literature concerning feature selection delineates three primary approaches: (i) Filter methods, such as univariate feature selection and correlation-based feature selection, prioritize features based on specific scores; (ii) Wrapper methods, exemplified by evolutionary algorithms and branch-and-bound algorithms, identify optimal feature subsets through search strategies in conjunction with predictive models; (iii) Embedded methods, including Least Absolute Shrinkage and Selection Operator (LASSO) [14] and Decision Tree (DT), integrate feature selection into the optimization goals of predictive tasks. However, each approach manifests both strengths and limitations. For instance, filter methods may neglect dependencies among features and the interaction between feature selection and predictors, while wrapper methods encounter challenges in exploring an extensive feature space with 2^N potential feature subsets for N features. Embedded methods heavily rely on structured assumptions inherent in predictive models. Consequently, effective feature selection demands a comprehensive approach that encompasses: (i) strategic assessment of feature importance, (ii) efficient exploration for an optimal feature subset, and (iii) seamless integration with predictive models. The current research on the fusion of EEG signal brainwave characteristics encompasses diverse methodologies, including linear combination methods [15] and approaches that amalgamate general Machine Learning (ML), specifically with Deep Learning (DL) [16].

Meanwhile, in recent years, Explainable Artificial Intelligence (XAI) has emerged as one of the most prominent topics aimed at addressing the explainability of ML and, in particular, DL methods, as well as developing strategies to enhance the explainability of ML algorithm outcomes. Generally, explainable methods [17] are of two types: antehoc and post-hoc. For ante-hoc, it is usually incorporated directly into the model structure, such as linear regression; for post-hoc, it explains the results of the model predictions based on what is easy to explain. Among them, classical permutation-based algorithms are usually used in combination with ML, such as Permutation Feature Importance (PFI) [18]. In addition, there are advanced local agent methods that aim to replace decision functions with directly explainable local agent models (e.g., SHapley Additive exPlanations (SHAP) [19].

Therefore, to enhance feature selection performance and achieve higher accuracy with a streamlined set of features,

we propose a novel ALO-MARL-based EEG feature selection algorithm. This algorithm, integrated with ML classifier parameter optimization for depression recognition, facilitates a balanced approach to global and local search. Concurrently, in order to post-interpret the model, we utilize XAI methods based on post-hoc approaches to directly explain trained models, elucidating the relationship between depression features and recognition. This provides an ideal method for the auxiliary diagnosis of depression in patients, without the need for adjusting internal parameters of the chosen classification model.

The main contributions of this work can be summarized as follows: we extract linear and non-linear EEG features. Subsequently, we propose a novel algorithm for EEG feature selection, coupled with ML classifier parameter optimization for depression detection. This approach achieves highly effective depression recognition with a reduced feature set. Finally, we use two different XAI approaches [20] and a TDE-HMM model to focus on the interpretation of the classification results of the model.

II. MATERIALS AND METHODS

A. Data Acquisition and Preprocessing

In this work, the EEG signals under audio stimulation are collected by electrodes located on the prefrontal-lobe (Fp1, Fpz, and Fp2) using a wearable three-lead EEG device developed by the Key Laboratory of Brain Health Intelligent Evaluation and Intervention (Beijing Institute of Technology, China) [3], [21], as shown in Fig. 1. In addition, two other electrodes are placed on two mastoid processes (A1 and A2) as reference and bias electrodes, respectively. All electrodes are placed according to the 10-20 international electrode placement systems [22]. In particular, we employ six auditory stimuli characterized by different emotional properties to investigate differences between depressed patients and healthy controls. The first two stimuli were neutral in nature, followed by two stimuli with negative emotional valence, and concluding with two stimuli characterized by positive emotional valence [12].

We recruited 70 depressed patients (16 to 56 years old) and 108 healthy controls (18 to 55 years old) from psychiatric hospitals for the experiment. All participants were carefully examined and screened by a professional psychiatrist using the Patient Health Questionnaire-9 (PHQ-9). Prior to data collection, participants were given a full explanation about the study and assured that their private data would not be disclosed. Each subject volunteered to participate in the study after being fully informed about the work and signing an informed consent form with their legal guardians. The consent forms and study design were approved by the local Ethics Committee for Biomedical Research at the Lanzhou University Second Hospital, and the ethics approval number is 2022A-620. In addition, all subjects are not taking any medication and are free from diseases such as epilepsy and other neurological abnormalities.

The experimental paradigm, as illustrated in Fig. 1, involved each participant undergoing a 72 s auditory stimulus experiment, followed by the analysis of the collected EEG data.

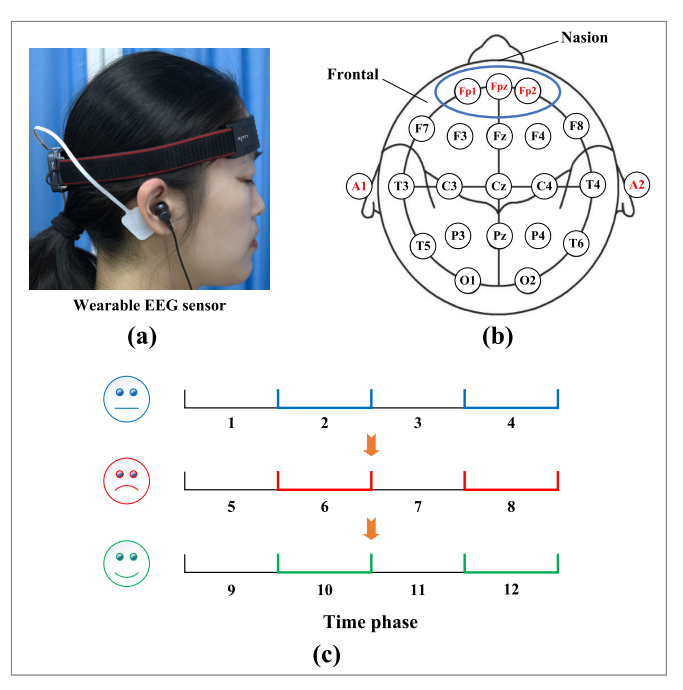


Fig. 1. The paradigm of the audio stimulation experiment. EEG signals induced by different audio stimuli are recorded using a wearable three-lead EEG sensor. (a) Wearable three-lead EEG sensor. (b) Three-lead EEG electrode locations in the prefrontal lobe. (c) The auditory stimulation process can be delineated into three major phases, namely neutral, negative, and positive stimuli. Furthermore, the stimulation protocol adopts an intermittent stimulation paradigm, interspersed with intervening resting phases.

The experiment is divided into 3 major phases and 6 minor phases, which can be further divided into 12 sub-phases at a smaller granularity. Firstly, in the first major phase, the subjects are in a resting state for 6 s, then, a neutrally-valenced audio stimulation is played for 6 s, paused for 6 s, and then repeated for 6 s, marking the end of this phase. The second and third major phases have a similar experimental procedure as the first phase, except that the type of audio played is different: negatively-valenced audio is played in the second major phase, and positively-valenced audio is played in the third major phase [12]. The stimulation audio is derived from the International Affective Digitized Sound (IADS-2) [23].

EEG signals are acquired using three-lead EEG sensors operating at a sampling frequency of 250 Hz. In the pursuit of maintaining data integrity, a Finite Impulse Response (FIR) filter is employed, characterized by a passband frequency spectrum spanning 0.1-45 Hz. The primary function of this filter is to eliminate prevalent issues such as baseline drift and Radio-Frequency Interference (RFI) noise. Due to the close proximity of electrodes to the ocular region, Ocular Artifacts (OAs) are inevitably captured by the sensors [24]. To address this challenge, a dual-method strategy is adopted, combining Discrete Wavelet Transformation (DWT) with a Kalman filter [3]. This approach is implemented to effectively expunge OAs from the EEG recordings, ensuring the purification and accuracy of the signal data.

B. Feature Extraction

The EEG signals are nonstationary and stochastic [25], and a single feature is inadequate to capture the diverse

and complex information they contain. Therefore, in this work, 7 features, including linear features (Mean-PSD, Max-PSD, and Min-PSD) and nonlinear features (FAA, LZC, SampEn, and REn), were extracted from the 72 seconds of audio-stimulated EEG data for feature selection.

- 1) Power Spectral Density (PSD): PSD has been shown to exhibit significant variation in relation to depression [3], [15], [26]. To leverage this relationship, three PSD-based features are extracted from the EEG signals: the mean (Mean-PSD), maximum (Max-PSD), and minimum (Min-PSD) values of the PSD. These features are selected to effectively capture the key characteristics of the PSD that are associated with depressive states.
- 2) Frontal Alpha Asymmetry (FAA): Asymmetric frontal activity serves as a crucial indicator of neurophysiological activity and is closely linked to emotional processing and affective disorders, such as depression [27], [28], [29]. FAA is computed by determining the difference in the PSD of the alpha rhythms between the Fp1 and Fp2 electrode sites. This measure has been widely utilized due to its association with frontal asymmetry and its relevance in studying depressive states.
- 3) Lempel-Ziv Complexity (LZC): LZC is a well-established metric in bioinformatics, particularly in the analysis of EEG signal complexity [30], [31], and has been successfully applied in EEG-based depression detection [3], [12]. Its utility lies in quantifying the complexity and irregularity of time series data, making it a valuable feature for assessing neural dynamics in relation to depressive states.
- 4) Sample Entropy (SampEn): SampEn, initially proposed by [32] for analyzing physiological time-series data, has been employed by [31] to evaluate EEG complexity across various depression severity levels and healthy control groups. This measure is particularly useful for capturing the irregularity and unpredictability of EEG signals, providing insight into the neural dynamics associated with depressive states.
- 5) Rényi Entropy (REn): Rényi Entropy is a generalization of Shannon entropy that introduces a parameter alpha, allowing for a more flexible assessment of uncertainty in probability distributions [33]. In EEG-based depression detection, it is used to quantify changes in brain activity complexity, as depression often leads to reduced neural signal complexity [34].

C. Feature Selection Through the ALO-MARL Algorithm

Feature selection is a common step in ML, which not only reduces feature redundancy, but also effectively improves the classification performance of the model. Various algorithms are currently employed to address the feature selection problem [35].

In this study, a wrapper approach [36] is employed to integrate feature selection into the model evaluation process, treating feature selection as the means to find the optimal solution for the model. The primary objective involves feature fusion, where a novel algorithm, termed the Ant Lion Optimization (ALO) - Multi-Agent Reinforcement Learning (MARL) algorithm, is introduced. This algorithm combines

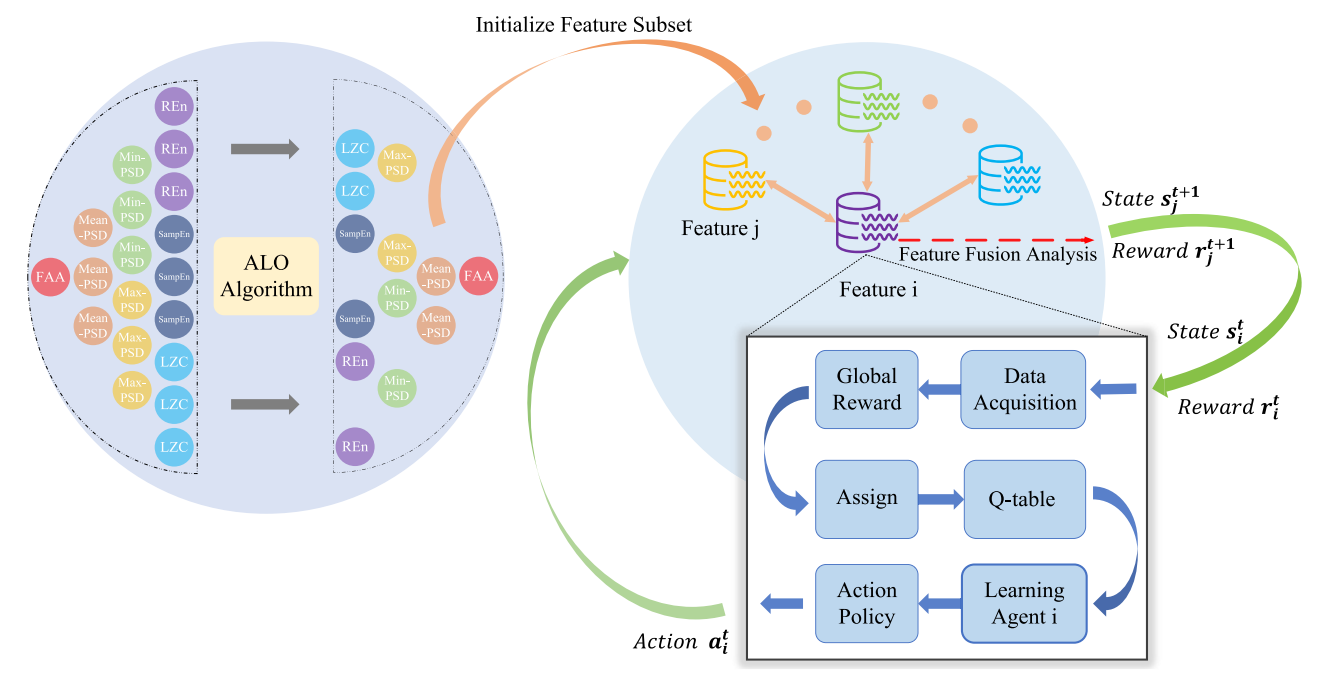


Fig. 2. Framework of the Proposed ALO-MARL algorithm. The left circle illustrates the feature selection process using the ALO algorithm, where initially, relevant features are selected from the original set of 19 features, forming a preliminary subset of features that are pertinent to the classification task. These pre-selected feature subsets are then fed into the subsequent MARL algorithm for further processing. The right side depicts a MARL framework containing multiple features, where each feature is treated as an agent that exchanges information with other features. Within the MARL framework, the agents iteratively optimize and update their states based on Global Rewards, ultimately identifying the optimal feature set.

the ALO and MARL algorithms, enhancing their effectiveness in depression recognition through the incorporation of parameter optimization techniques from ML classifiers [37], [38]. The ALO-MARL algorithm strives to strike a balance between global and local search methodologies to identify more optimal feature subsets for EEG feature selection. The algorithm is detailed in a comprehensive procedural framework, outlined in Algorithm 1, showcasing a synergistically enhanced effect resulting from the integration of the unique strengths of the ALO and MARL algorithms. Meanwhile, Fig. 2 illustrates the overall system framework, specifically the proposed ALO-MARL algorithm flowchart.

1) Feature Space Selection Based on the ALO Algorithm: The ALO algorithm is a nature-inspired metaheuristic based on the hunting behavior of antlions [39]. ALO simulates how antlions trap ants in sand pits, representing a search process to find optimal solutions in complex problem spaces. In ALO, each "ant" (a potential solution) performs a random walk around an "antlion" (a candidate best solution), which helps it explore different regions of the search space. This process is designed to balance exploration (finding new areas of the solution space) and exploitation (refining solutions in promising areas). In feature selection, ALO is used to identify the most relevant subset of features that maximizes classifier accuracy while reducing computational load [40].

The algorithm works in iterations, where each ant's movement is influenced by the closest antlion. The random walk can be represented as:

$$W_t = \sum_{i=1}^t (2r - 1) \tag{1}$$

where r is a random binary variable (either 0 or 1), creating a cumulative path influenced by the random choices.

As the algorithm progresses, the search radius around each antlion is gradually reduced, trapping ants closer to antlions over time, mimicking the natural shrinking effect in sand traps:

$$g_t = g_i/I, h_t = h_i/I \tag{2}$$

where I is an adaptive ratio that controls explorationexploitation, and g and h are the boundaries within which ants move. ALO's adaptive nature in shrinking the search space ensures efficient and accurate feature selection, particularly in high-dimensional data.

ALO includes an elitism strategy that ensures the best solution is retained across iterations, providing stability and improving convergence. The Blend Crossover Operation (BLX) is used to generate new candidate solutions around the best antlion. This crossover helps maintain diversity and prevent premature convergence, allowing ALO to be effective for a range of optimization tasks, especially for feature selection.

In this work, we utilize the ALO algorithm for feature selection to obtain an initial subset of features for subsequent algorithmic operations. Concurrently, the integration of a BLX can be incorporated to augment the search capability of the ALO algorithm, thereby yielding superior feature selection outcomes. The pseudocode of the ALO algorithm is presented in [3]. The fitness function used in this study is the F1-score.

2) Introduction to the Multi-Agent System Model: In the context of a solitary agent system, the reward function exclusively evaluates the states of two nodes, disregarding others. Consequently, it fails to capture the intricate interplay between the

```
Algorithm 1 Feature Selection Using the ALO-MARL Algorithm
```

```
Input: Training data (D), Maximum Iterations (N),
          Population Size (P)
   Output: Final feature subset (S), Model recognition
            effect (E)
1 begin
       Initialize: Randomly generate positions of ants (AN)
2
       and antlions (AL). Evaluate fitness of each ant's
       position using the objective function (e.g., classifier
       performance).
       for iter = 1 : N do
3
4
          for i = 1 : P do
               Perform random walk influenced by the
5
               position of the corresponding antlion.
               Update ant's position based on the random
               walk.
               Evaluate the fitness of the new position.
               Select the best ants (elite solutions) and
               update antlion positions: Replace antlions
               with the best-performing ants.
               If a better feature subset is found: Update the
9
              global best solution.
          end
10
11
       end
       Obtain the initial optimal feature subset.
12
       Initialize Q-values: \forall a \mid Q(a) = -1.
13
       for episode = 1 : num \ episodes \ do
14
          for agent = 1: num agents do
15
               if flag\ CLEAN == 1 then
16
                   Execute greedy (online) action a_i \in \{0, 1\}.
17
               else
18
                   Execute \epsilon-greedy action a_i \in \{0, 1\}.
19
               end
20
           end
21
22
           Observe joint action a. Get subset S by
           considering only "on" actions. Get global reward
           G(a) = Reward(S, D).
           for agent = 1 : num\_agents do
23
               if flag\ CLEAN == 1 then
24
25
                   Take \epsilon-greedy (offline) action c_i \in \{0, 1\}.
                   Calculate C_i = G(a - a_i + c_i) - G(a).
26
                   Update Q(c_i) \leftarrow Q(c_i) + \alpha [C_i - Q(c_i)].
27
               else
28
29
                   Update
                   Q(a_i) \leftarrow Q(a_i) + \alpha [G(a) - Q(a_i)].
              end
30
31
           end
32
          Reduce \alpha using \alpha_decay_rate. Reduce \epsilon using
           \epsilon\_decay\_rate.
```

environment and multiple agents within the system. In order to rectify this limitation, we present a novel multi-agent system model.

end

33

34 end

Fig. 2 illustrates a framework comprising multiple features, with each feature considered as an agent engaged in information exchange with others. Notably, the entire process of feature fusion analysis is conceptualized as a Markov Decision Process (MDP). Serving as the foundational theory for the Reinforcement Learning (RL) algorithm, MDP inherently captures the stochastic fluctuations in environmental states and addresses the stochastic optimization of the system objective. The implementation of this framework is supported by the incorporation of ALO-MARL models [41].

Moreover, within the framework of feature fusion analysis, all feature states collectively constitute the set of states denoted as S. At a specific time t, the state of the current feature i is represented as s_i^t . Additionally, the actions associated with the selection of feature i form the set of actions denoted as A_i , where the selection of feature i at time t is considered as the action a_i^t . Upon executing the action a_i^t , the resulting reward r_i^t is obtained as feedback. Furthermore, leveraging the insights from feature fusion analysis, the determination of the Global Reward at time t transpires. Subsequently, the Global Reward is distributed among agents through an assignment mechanism. Ultimately, the decision-making process for feature fusion analysis is executed, leading to the selection of features essential for the model. The definition and assignment of Global Reward will be discussed in detail later.

Significantly, the information interactions among agents play a pivotal role in enabling feature fusion analysis to respond promptly to dynamic environmental changes. Building upon this foundation, the present agent computes the associated reward and *Q*-value based on the available information, ultimately selecting an action through comparative analysis.

From the model elucidated above, it becomes evident that an anticipated trajectory is obtained through iterative information interactions and continuous adjustments. Broadly speaking, the resolution to the MDP problem lies in the application of the *Q*-learning algorithm. In *Q*-learning, the experience of the agent is encapsulated within a sequence of discrete episodes, facilitating the learning of an optimal strategy without necessitating knowledge of the detailed MDP model at each step. Serving as the bedrock for the implementation of RL-based feature fusion analysis, the foundational formula is as follows:

$$\begin{aligned} Q_{i}^{t+1}(s_{i}^{t}, a_{i}^{t}) &= (1 - \alpha) Q_{i}^{t}(s_{i}^{t}, a_{i}^{t}) \\ &+ \alpha \left\{ r^{t+1}(s_{j}^{t+1}) + \gamma * \max_{\alpha \in A_{j}} Q_{j}^{t}(s_{j}^{t+1}, a) \right\}, \end{aligned}$$
(3)

where α denotes the learning rate, and γ serves as a discount factor. $Q_i^t(s_i^t, a_i^t)$ is defined as a Q-function designed to estimate the Q-value, representing the cumulative reward when an agent takes action $a_i^t \in A_i$ in state $s_i^t \in S$. Simultaneously, $r^{t+1}(s_j^{t+1})$ signifies the immediate reward at time t+1 when an agent transitioning from state s_i^t to s_i^{t+1} .

3) Reward Function for RL: The presented approach aligns with the concept of multiple information learners, where each agent views other agents as integral components of the environment, contributing to its dynamic nature through interactions [42]. The methodology employs a Global Reward

as the main feedback signal, derived from an aggregate evaluation of all agents. However, this reward is susceptible to perturbations from other agents' exploratory actions, posing a challenge in distinguishing disturbances from environmental dynamics or other agents' actions. To address this, the CLEAN rewards [43] method is adopted, representing the difference between the global reward under exploratory actions and a greedy strategy.

In the context of feature selection, the approach treats it as a multi-agent coordination challenge, assigning a dedicated learning agent to each feature. The goal is to filter out irrelevant features, and each agent decides on the inclusion or exclusion of a specific feature. Actions 0 and 1 denote deactivation and activation of a feature, respectively, forming the feature subset. The reward function is framed as a multi-objective problem, aiming to simultaneously reduce the subset size and improve classification performance, considering metrics like accuracy or F1-score. A penalty is introduced when the subset size exceeds a predetermined upper limit. The reward function is defined in:

$$Reward = \begin{cases} P, & s \le k \\ P \cdot k/s, & s > k \end{cases} \tag{4}$$

with k representing the maximum permissible features, s indicating the subset size, and P representing its corresponding classification performance.

D. Explainable Artificial Intelligence (XAI)

The computational cost of the PFI is low, SHAP is capable of providing explanations for the overall model with consistency and high credibility. Hence, we are employing these two methods for post-model interpretation. These two different methods are applied to interpret the model classification and quantify feature importance. The following content provides a more in-depth description of the above explainable methods.

- 1) Permutation Feature Importance (PFI): This method is based upon Mean Reduction Accuracy, and it can be used as an alternative method to overcome the drawbacks of calculating the default feature importance with the Mean Decrease in Impurity. It measures the changes in model prediction error (in our case cross-entropy loss) when a single feature value is randomly disrupted. The variation in the model score shows how much the model depends on the feature [44]. In fact, permuting important features leads to a considerable decrease in accuracy, while the effect of permuting less relevant features should be negligible [18].
- 2) SHapley Additive exPlanations (SHAP): This is a model-agnostic interpretation method that belongs to the additive feature attribution approach, which builds on the game-theoretic concept of Shapley values. These values are used to determine the contribution of each player in a coalition or a cooperative game. In fact, initially, Shapley [45] proposed a game-theoretic approach that assigns fair payoffs to players based on their contributions to the total payoff. In a prediction task, this corresponds to assigning quantitative values to each feature based on its contribution to a particular prediction. The SHAP method calculates the Shapley values and represents them as a linear model of feature coalitions [46].

According to [19], SHAP values attribute to each feature the change in the expected model prediction when the condition is applied to that feature. In this framework, the difference between the prediction and the average prediction, which is considered as the baseline reference, is perfectly distributed among all features. Thus, the SHAP values for all features add up to explain the difference between the actual prediction and the baseline. The SHAP method is quite robust and it yields a comparative interpretation of individual predictions versus average predictions.

E. Time-Delay Embedded Hidden Markov Model (TDE-HMM)

TDE-HMM showcases distinct advantages in the analysis of internal state transitions within EEG data through the utilization of time-delay embedding and Hidden Markov Modelling techniques. This approach provides enhanced temporal representation, robustness, and adaptability tailored to the inherent characteristics of EEG data.

As a general framework, a Hidden Markov Model (HMM) assumes that a time series can be described using a hidden sequence of a finite number of states such that at each point in time, only one state is active. In practice, since the HMM is a probabilistic model, there is uncertainty in the inference process, assigning the probability of being active at each time point to each state [47]. The HMM is an effective method for analyzing state transitions and can be used for state and transition probability estimation. It has been widely used for modelling multi-channel neural data [48].

For traditional HMMs, the observation function may have a large number of parameters, which may lead to overfitting. As a result, this makes the HMM unable to segment time series effectively. Here, we apply a novel HMM to the original time series, which allows us to detect changes not only in power but also in phase-locking.

In this approach, the TDE-HMM, we define the observation distribution as the neural activity over a specific time window. We use a Gaussian distribution with zero mean (i. e., using the covariance matrix) to model the entire window. To avoid extensive computation and severe overfitting problems, we run the HMM on a Principal Component Analysis (PCA) decomposition of the embedded space, which not only greatly reduces the complexity of the state distribution, but also naturally concentrates the slower frequencies in the data. Therefore, besides the number of states, the important parameters of the model are the length of the window (i. e., the number of lags to be modelled by the state autocovariance matrices) and the number of PCA components [48].

III. EXPERIMENTS AND RESULTS

A. Experimental Settings for Experimental Testing of the Recognition Model

In this work, six features (Mean-PSD, Max-PSD, Min-PSD, LZC, SampEn, and REn) are extracted from each of the three EEG channels (Fp1, Fpz, and Fp2), resulting in a total of 3*6=18 features. Additionally, the feature FAA is calculated based on the difference in the PSD of the alpha

rhythms between the Fp1 and Fp2 electrode sites, serving as an additional feature dimension. Therefore, a total of 19 features are used for feature selection and analysis in the ALO-MARL algorithm.

This paper explores three strategies for feature fusion analysis in the context of depression recognition tasks. These strategies include a novel approach proposed by us, namely the ALO-MARL algorithm for feature fusion analysis, the independent application of the ALO algorithm for feature selection, and the independent use of MARL for feature selection. In the first strategy, the process involves the initial screening of feature subsets using the ALO algorithm to obtain an initialized feature subset. Subsequently, this subset is modeled using the MARL algorithm for feature fusion analysis, followed by the optimization of ML classifier hyper-parameters through a grid search strategy and ultimately concluding with depression recognition.

The ALO-MARL algorithm is run for different values for k, i. e., the number of features we wish to include in the model. The value of the upper boundary on the number of features to be included in the model is varied from 5 to n (i. e., the size of the initial screening feature subset). Further, for our method using RL, we fixed the parameters $\alpha=0.2$, $\epsilon=0.5$, α decay rate = 0.995, and ϵ decay rate = 0.995. The number of episodes we train our model is kept to 100. In addition, the number of independent executions is set to 10. Furthermore, independent executions are performed to avoid random results of a particular classifier.

The details of the parameter settings of the ALO algorithm are kept fixed in each independent execution to obtain the results. In addition, the population size (i.e., the number of independent executions) and the maximum number of iterations are set to 20 and 100, respectively [3]. Additionally, we utilize a 10-fold cross-validation approach to evaluate the model's performance. This method entails dividing the training dataset into 10 subsets, reserving one for model validation and employing the remaining nine for training. The procedure is executed ten times, yielding ten distinct models. The overall model performance is determined by averaging the results obtained from these ten iterations.

B. Classification Methods

To validate the effectiveness of the feature selection methods, this study employs several classical ML methods for classification, which are commonly used in affective computing and emotion recognition. A total of 6 classifiers are used to obtain the classification results.

- 1) *k*-Nearest Neighbor (*k*-NN): As a widely used instance-based and supervised ML algorithm, *k*-NN is commonly applied in both classification and regression tasks [49]. In this study, the ALO-MARL algorithm was utilized to identify the optimal value of k, enhancing classification performance.
- 2) Support Vector Machine (SVM): SVM, grounded in statistical learning theory, is a supervised ML algorithm known for its low computational complexity and strong classification capabilities [3]. In this study, an SVM classifier with a Radial Basis Function (RBF) kernel was employed.

- 3) Naive Bayes (NB): NB is one of the simplest forms of Bayesian network classifiers and is a supervised ML algorithm commonly applied to classification tasks [50].
- 4) Decision Tree (DT): DT is a nonparametric, supervised ML method used for both classification and regression tasks, offering high classification accuracy and robust performance [51].
- 5) Random Forest (RF): RF is a supervised ML algorithm that performs well across a wide range of classification and regression tasks [52].
- 6) XGBoost: XGBoost is an ensemble ML algorithm based on decision trees, utilizing a Gradient Boosting framework to enhance performance [53].

C. Comparison With Different Feature Selection Methods Based on Different Classifiers

In this study, the proposed ALO-MARL algorithm is systematically compared with both traditional and state-ofthe-art feature selection methods. Traditional methods include LASSO [14], Correlation-Based Feature Selection (CFS) [54], RF [52], Infinite Feature Selection (IFS) [55], ReliefF [56], Fisher Score [57], Information Gain (InfoGain) [58], Support Vector Machine-Recursive Feature Elimination (SVM-RFE) [59], and Genetic Algorithm (GA) [60], all of which are widely employed in prior research. In addition, the study evaluates the ALO-MARL algorithm against several recent state-of-the-art techniques, such as Standard Deviation and Exponent Cosine Similarity-Based Feature Selection (SCEFS), Standard Deviation and Reciprocal Cosine Similarity-Based Feature Selection (SCRFS) and Standard Deviation and Anti-Cosine Similarity-Based Feature Selection (SCAFS) [61]. These methods represent advancements in feature selection and provide a broader context for comparison.

The methods are categorized based on their selection strategy: embedded, filter, and wrapper approaches. Embedded methods include LASSO, SVM-RFE, and RF, which incorporate feature selection as part of the model training process. Filter methods, such as Fisher Score, CFS, InfoGain, ReliefF, IFS, SCEFS, SCRFS, and SCAFS, evaluate features independently of the model using statistical criteria. Wrapper methods, including GA, ALO, MARL, and the proposed ALO-MARL algorithm, involve iterative optimization to identify the best subset of features. All traditional methods are implemented using Python's Feature Selection Library within the PyCharm environment, employing their respective default parameter settings.

Tables I-VI present the classification results for distinguishing between normal and depressed subjects using different feature selection methods and classifiers. Among the six classifiers and various feature selection strategies, the wrapper-based feature selection method consistently yields the best classification performance, particularly in terms of F1-score, accuracy, sensitivity, and specificity. Notably, within the wrapper-based feature selection methods, our proposed ALO-MARL algorithm demonstrates superior performance across all evaluation metrics, underscoring its effectiveness in both feature selection and classification tasks.

TABLE I

EVALUATION OF DEPRESSION RECOGNITION PERFORMANCE OF
DIFFERENT FEATURE SELECTION METHODS BASED ON k-NN
CLASSIFIER (MEAN±SD%)

Method	F1-score	Accuracy	Sensitivity	Specificity	
Baseline	85.07±3.42	89.54±2.21	76.47±5.00	97.87±1.45	
LASSO	84.75±5.06	89.26±2.99	77.24±6.26	96.87±2.28	
SVM-RFE	84.94±4.57	89.47±2.54	76.89±5.72	97.43±1.46	
RF	85.63±4.21	89.89±2.26	77.94±5.05	97.45±1.68	
Fisher	85.08±3.57	89.54±2.11	76.93±5.13	97.55±1.63	
CFS	85.08±3.57	89.54±2.11	76.93±5.13	97.55±1.63	
InfoGain	85.20±4.09	89.68±2.43	76.90±5.86	97.78±1.71	
ReliefF	85.07±3.76	89.54±2.51	76.50±5.27	97.87±1.45	
IFS	84.62±2.27	89.11±1.68	76.39±3.61	97.30±1.72	
SCEFS	83.33±4.38	88.35±2.67	74.92±5.50	97.01±1.73	
SCRFS	78.56±3.54	85.25±2.55	68.97±4.47	95.81±1.13	
SCAFS	83.33±4.38	88.35±2.67	74.92±5.50	97.01±1.73	
GA	84.93±1.85	89.40±0.94	76.50±3.73	97.65±1.55	
ALO	88.19±0.34	91.21±0.34	83.88±1.61	95.96±1.40	
MARL	88.20±0.62	62 91.89±0.33 80.76±1.98		98.60±1.17	
ALO-MARL	91.09±0.25	93.68±0.24	85.19±0.75	98.87±0.80	

Baseline: without feature selection; LASSO: Least Absolute Shrinkage and Selection Operator; SVM-RFE: Support Vector Machine-Recursive Feature Elimination; CFS: Correlation-based Feature Selection; InfoGain: Information Gain; IFS: Infinite Feature Selection; SCEFS: Standard Deviation and Exponent Cosine similarity-based Feature Selection; SCRFS: Standard Deviation and Reciprocal Cosine similarity-based Feature Selection; SCAFS: Standard Deviation and Anti-Cosine similarity-based Feature Selection.

TABLE II

EVALUATION OF DEPRESSION RECOGNITION PERFORMANCE OF
DIFFERENT FEATURE SELECTION METHODS BASED ON SVM
CLASSIFIER (MEAN±SD%)

Method	F1-score	Accuracy	Sensitivity	Specificity
Baseline	83.67±2.78	88.69±2.02	73.89±3.50	98.25±1.65
LASSO	83.79±2.78	88.69±1.87	74.77±3.64	97.69±1.36
SVM-RFE	83.26±2.94	88.48±1.81	73.47±3.73	98.17±1.54
RF	83.16±3.54	88.34±2.26	73.85±4.53	97.69±1.35
Fisher	83.27±2.94	88.48±2.11	73.18±3.88	98.36±1.50
CFS	83.27±2.94	88.48±2.11	73.18±3.88	98.36±1.50
InfoGain	83.31±2.93	88.55±1.87	73.12±3.90	98.49±1.63
ReliefF	83.75±2.92	88.76±1.99	74.06±3.81	98.27±1.63
IFS	83.53±2.75	88.62±1.93	73.71±3.49	98.27±1.47
SCEFS	81.14±2.69	87.15±1.90	70.55±3.70	97.93±1.50
SCRFS	77.13±4.71	84.62±3.11	66.38±5.33	96.40±2.04
SCAFS	81.14±2.69	87.15±1.90	70.55±3.70	97.93±1.50
GA	83.10±3.10	88.41±1.77	73.10±4.57	98.28±0.88
ALO	84.27±0.07	88.99±0.07	.99±0.07 75.55±0.31 9	
MARL	80.42±0.05	5 86.28±0.11 68.63±0.77		98.57±0.71
ALO-MARL	91.32±0.45	93.33±0.23	86.96±0.94	97.65±0.27

In this study, we focus primarily on three algorithms: the ALO, MARL, and the proposed ALO-MARL algorithm, which are employed for feature fusion analysis. After performing feature selection using these algorithms, we optimize the hyper-parameters of a ML classifier to effectively identify individuals with depression. This process enables the accurate recognition of depression in individuals.

TABLE III

EVALUATION OF DEPRESSION RECOGNITION PERFORMANCE OF DIFFERENT FEATURE SELECTION METHODS BASED ON NB CLASSIFIER (MEAN±SD%)

Method	F1-score	Accuracy	Accuracy Sensitivity	
Baseline	58.75±6.90	44.15±13.85	97.12±8.65	9.23±27.69
LASSO	58.75±6.90	44.15±13.85	97.12±8.65	9.23±27.69
SVM-RFE	76.53±3.74	83.50±2.95	68.44±3.33	93.27±2.61
RF	76.82±3.34	83.78±2.65	68.44±3.28	93.73±2.13
Fisher	76.17±3.73	83.22±2.97	68.24±3.24	92.91±2.71
CFS	76.17±3.73	83.22±2.97	68.24±3.24	92.91±2.71
InfoGain	59.69±6.62	47.39±12.91	95.22±8.26	15.90±25.75
ReliefF	77.01±4.42	83.29±3.52	71.29±4.68	91.05±3.05
IFS	73.85±4.56	81.53±3.37	66.44±4.45	91.29±3.18
SCEFS	58.65±6.54	44.16±13.60	96.92±9.23	9.34±27.66
SCRFS	74.73±4.64	81.53±3.78	69.40±4.97	89.40±3.46
SCAFS	58.65±6.54	44.16±13.60	96.92±9.23	9.34±27.66
GA	76.92±3.10	83.64±1.77	69.35±4.57	92.93±0.88
ALO	77.85±0.20	84.38±0.29	±0.29 70.30±1.14 93	
MARL	79.76±0.39	84.60±0.29	60±0.29 72.08±1.00 93	
ALO-MARL	80.14±0.36	86.46±0.28	72.13±0.50	95.20±0.52

TABLE IV

EVALUATION OF DEPRESSION RECOGNITION PERFORMANCE OF DIFFERENT FEATURE SELECTION METHODS BASED ON DT CLASSIFIER (MEAN±SD%)

Method	F1-score	Accuracy	Accuracy Sensitivity	
Baseline	80.05±3.57	84.35±2.30	80.28±6.09	86.82±3.38
LASSO	80.72±4.29	84.62±2.53	82.49±4.89	85.85±2.62
SVM-RFE	81.01±5.34	85.12±3.37	81.52±5.97	87.44±3.09
RF	79.69±4.48	84.13±2.56	80.33±6.26	86.43±2.98
Fisher	79.46±3.81	84.06±1.84	79.18±5.90	87.13±2.63
CFS	79.07±2.73	83.71±1.54	78.83±4.29	86.73±2.48
InfoGain	80.33±3.78	84.83±2.66	80.03±6.22	87.79±3.50
ReliefF	80.28±2.16	84.63±1.62	80.02±3.85	87.38±3.07
IFS	82.33±3.83	86.24±2.20	81.71±5.56	89.03±1.78
SCEFS	76.38±3.16	81.47±2.13	76.78±4.67	84.40±4.02
SCRFS	72.50±4.90	78.44±3.45	73.17±7.89	81.66±4.61
SCAFS	77.55±3.88	82.45±3.24	77.18±3.94	85.72±4.69
GA	80.79±3.51	85.18±2.46	79.85±3.37	88.58±2.98
ALO	83.95±0.47	87.42±0.38	83.68±0.74	89.84±0.53
MARL	85.55±0.50	88.88±0.47	80.86±1.96	94.38±1.80
ALO-MARL	87.92±0.51	90.46±0.41	86.09±1.10	93.41±0.86

The feature selection process using the ALO algorithm is performed independently in each execution, with different feature subsets selected for training. The results of 20 independent executions are averaged to provide the final performance of the classifier. As shown in Tables I-VI, all six classifiers achieve strong results, with *k*-NN and XGBoost showing the best performance. Specifically, *k*-NN achieves an F1-score of 88.19% and accuracy of 91.21%, while XGBoost reaches an F1-score of 88.18% and accuracy of 91.24%.

For feature fusion analysis using the MARL algorithm, a total of 10 independent experiments are conducted. In each experiment, a feature subset is selected for a particular classifier, and the classifier's performance is evaluated. The results, presented in Tables I-VI, show that the XGBoost classifier outperforms the others, achieving an F1-score of 90.02%,

² Bold represents the optimal classification results for three primary feature selection approaches.

TABLE V

EVALUATION OF DEPRESSION RECOGNITION PERFORMANCE OF DIFFERENT FEATURE SELECTION METHODS BASED ON RF CLASSIFIER (MEAN±SD%)

Method	F1-score	Accuracy	Sensitivity	Specificity	
Baseline	82.88±3.37	87.92±2.11	74.82±3.92	96.25±1.94	
LASSO	85.08±2.66	89.40±1.59	77.66±4.82	96.81±2.00	
SVM-RFE	84.40±2.51	88.91±1.53	76.85±3.64	96.60±1.12	
RF	84.57±2.48	89.12±1.17	76.63±3.19	97.12±1.13	
Fisher	83.91±3.27	88.70±2.07	75.53±5.05	97.02±2.09	
CFS	83.44±4.03	88.42±2.38	75.02±5.93	96.93±1.94	
InfoGain	84.21±3.51	88.77±2.36	76.31±4.66	96.70±2.12	
ReliefF	84.44±1.91	88.91±1.59	76.67±2.64	96.68±2.02	
IFS	85.60±3.55	89.75±2.33	77.98±4.61	97.31±1.78	
SCEFS	84.51±3.39	88.84±2.78	77.26±4.23	96.38±2.11	
SCRFS	77.32±4.37	84.05±2.88	69.53±4.65	93.38±3.04	
SCAFS	84.51±3.39	88.84±2.78	88.84±2.78 77.26±4.23		
GA	84.32±3.24	88.69±1.87	77.69±4.17	95.63±1.66	
ALO	86.65±0.38	90.44±0.27	79.57±0.55	97.49±0.42	
MARL	86.36±0.73	90.11±0.52	79.73±0.98	96.82±0.53	
ALO-MARL	91.30±0.23	92.98±0.16	85.37±0.64	98.77±0.46	

TABLE VI
EVALUATION OF DEPRESSION RECOGNITION PERFORMANCE OF
DIFFERENT FEATURE SELECTION METHODS BASED ON XGBOOST
CLASSIFIER (MEAN±SD%)

Method	F1-score	Accuracy	Sensitivity	Specificity	
Baseline	86.56±3.84	90.24±2.14	81.31±4.67	95.83±1.93	
LASSO	85.54±2.45	89.33±1.52	80.93±3.92	94.63±1.72	
SVM-RFE	86.87±3.61	90.31±2.44	82.18±4.92	95.42±2.19	
RF	86.03±3.68	89.75±2.46	81.04±4.05	95.21±2.42	
Fisher	86.04±3.49	89.75±2.03	81.53±4.42	94.89±1.71	
CFS	86.19±3.39	89.89±1.91	81.53±4.42	95.12±1.60	
InfoGain	86.91±4.80	90.38±2.94	82.27±5.12	95.46±2.69	
ReliefF	87.72±2.59	91.01±1.55	82.46±3.33	96.38±1.97	
IFS	87.30±3.45	90.66±2.07	82.85±4.64	95.59±1.67	
SCEFS	84.09±3.17	88.27±2.51	79.04±3.70	94.14±2.07	
SCRFS	79.37±4.54	84.76±2.93	75.32±6.20	90.68±3.14	
SCAFS	84.09±3.17	88.27±2.51	79.04±3.70	94.14±2.07	
GA	85.81±2.85	89.40±1.55	82.36±4.38	93.80±1.29	
ALO	88.18±0.37	91.24±0.27	83.54±0.56	96.24±0.35	
MARL	90.02±0.38	92.21±0.31	85.56±0.71	96.85±0.60	
ALO-MARL	91.82±0.26	93.69±0.18	88.60±0.65	97.08±0.27	

accuracy of 92.21%, sensitivity of 85.56%, and specificity of 96.85%. In contrast, the NB classifier demonstrates the worst performance, with an F1-score of 79.76%, accuracy of 84.60%, sensitivity of 72.08%, and specificity of 93.70%.

Finally, when applying the ALO-MARL algorithm for feature fusion analysis, the process begins with initial feature subset screening using the ALO algorithm. This subset serves as the starting point for the subsequent RL process. The feature selection problem is framed as an RL task, where each feature is treated as an agent. The actions taken by each agent are binary (0 or 1), where 0 indicates exclusion and 1 indicates selection. Through interaction between the agents and the environment, the optimal feature set is obtained, resulting in improved classification performance.

TABLE VII

AVERAGE SIZE OF THE FEATURE SUBSETS FOR DIFFERENT METHODS

OF FEATURE SELECTION (TIMES)

Method	k-NN	SVM	NB	DT	RF	XGBoost
ALO	16.0	11.0	13.0	15.0	14.0	16.0
MARL	12.2	12.2	10.6	15.0	12.6	14.7
ALO-MARL	12.2	9.0	9.6	12.2	12.0	11.0

As shown in Tables I-VI, the ALO-MARL method significantly enhances classification performance. The XGBoost classifier achieves the highest results with an F1-score of 91.82%, accuracy of 93.69%, sensitivity of 88.60%, and specificity of 97.08%. In contrast, the NB classifier again shows the worst performance, with an F1-score of 80.14%, accuracy of 86.46%, sensitivity of 72.13%, and specificity of 95.20%.

Table VII presents the feature subset lengths for the three feature selection methods across the six classifiers. The ALO-MARL method consistently selects smaller feature subsets for each classifier, which not only leads to reduced model complexity but also results in better recognition performance. This demonstrates that the ALO-MARL method can achieve superior classification results with a more compact set of features.

The above analysis indicates that our proposed approach, utilizing the ALO-MARL algorithm for feature fusion analysis, along with the optimization of ML classifier parameters, is the most effective for depression recognition.

In the case of using the ALO-MARL algorithm for feature selection while simultaneously using the XGBoost classifier for depression recognition, after conducting 10 independent executions, we exclude 8 features from the model and retain 11 features. These features include the Mean-PSD in all 3 leads, the Max-PSD in the second lead, the Min-PSD in the first and third leads, the SampEn in all 3 leads, and the REn in the first and second leads. We utilize these features to improve the classification results of the model. Later, we utilize these features to improve the classification effect of the model and perform post-model explanations.

The results of the XGBoost classifier parameter optimization are: the values of colsample_bytree, gamma, max_depth, min_child_weight, and n_estimators equal 0.8, 0.5, 7, 3, and 100.

Table VII presents the average size of the feature subsets obtained after conducting multiple feature selection experiments using the ALO, MARL, and ALO-MARL algorithms. The concurrent examination of Table VII reveals that the ALO-MARL method, in comparison to both the ALO and MARL approaches, is capable of achieving satisfactory recognition outcomes with a relatively reduced subset of features. Furthermore, for the six classifiers considered, the ALO-MARL algorithm exhibits a conspicuous enhancement in the identification performance for depression, particularly in the case of the SVM, DT, and RF classifiers. The various details pertaining to the optimization of model hyper-parameters are delineated in Table VIII.

	COMMANT OF MODEL THE ENTRICKMETERS
Classifiers	Model Hyper-parameters
k-NN	n_neighbors=3, weights="uniform", algorithm="auto", leaf_size=30, p=1, metric="minkowski"
SVM	C=5.0, kernel="rbf", degree=3, gamma="scale", coef0=0.0, tol=1e-3, cache_size=200, max_iter=-1, decision_function_shape="ovr"
NB	None
DT	criterion="gini", splitter="best", max_depth=None, min_samples_split=2, min_samples_leaf=1, min_weight_fraction_leaf=0.0, min_impurity_decrease=0.0
RF	n_estimators=10, criterion="gini", max_depth=None, min_samples_split=2, min_samples_leaf=2, min_weight_fraction_leaf=0.0, max_features="sqrt", max_leaf_nodes=None, min_impurity_decrease=0.0
XGBoost	colsample_bytree=0.8, gamma=0.5, max_depth=7, min_child_weight=3, n_estimators=100

TABLE VIII
SUMMARY OF MODEL HYPERPARAMETERS

D. Computational Complexity of Different Feature Selection Methods

We also analyze and compare the computational complexity of different feature selection methods. The computational time is calculated as the difference between the time when prediction ends after the feature subset is selected and the time before feature selection begins. All experiments are run on a computer with Windows 11 OS, a 13th Gen Intel(R) Core(TM) i7-13700F with 16 GB RAM.

As shown in Table IX, the proposed ALO-MARL algorithm demonstrates comparable, if not shorter, computation time compared to other wrapper-based feature selection methods, making it feasible to complete computations within a reasonable timeframe. However, due to the inherent computational inefficiency of wrapper-based methods, embedded and filter-based feature selection methods exhibit significantly shorter computation times than ALO-MARL.

Although ALO-MARL requires slightly more runtime than embedded and filter-based methods, the results in Tables I, II, III, IV, V, and VI reveal its superior performance metrics. The feature subsets selected by ALO-MARL significantly enhance model accuracy and generalization capability, highlighting its advantages in performance. This outstanding performance offsets the algorithm's runtime disadvantage, making ALO-MARL highly competitive in applications where high precision is required.

In conclusion, the ALO-MARL algorithm is a feature selection method that balances computational efficiency and performance effectively.

E. Results for the Model Explanations With the XAI Methods

From the analysis presented above, it is clear that the XGBoost model, enhanced by the ALO-MARL feature fusion algorithm, demonstrates the best performance in depression recognition. The following section delves into the post-interpretation results using XAI methods based on this model.

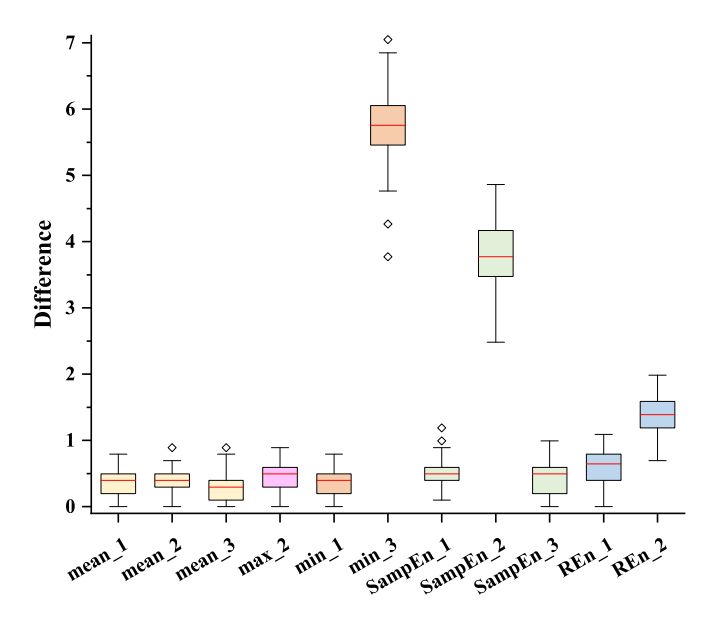


Fig. 3. Boxplot grouped by feature. The vertical coordinate is the value of the impact on the performance of the model after randomly shuffling the feature values. The horizontal coordinate is the features selected by the algorithm.

Fig. 3 illustrates the feature importance based on PFI technique. It is evident that among the various features considered, three features stand out in terms of their contribution to the model. Specifically, the minimum value of PSD in the third lead emerges as the most influential feature, followed closely by the SampEn in the second lead. This suggests that these features play a crucial role in distinguishing depression, as compared to the other features included in the analysis.

Additionally, the SHAP values provide further insight into the XGBoost model's decision-making process. The SHAP summary plot, shown in Fig. 4, serves as an alternative to the typical feature importance bar chart, offering a comprehensive overview of each feature's impact. The plot not only identifies the most significant features but also highlights the range of their effects across the dataset. Notably, the color gradients in the plot vividly reveal the correlation between variations in feature values and the corresponding changes in depression detection. Strong correlations are particularly observed between the PSD and SampEn features and their contribution to depression recognition.

Furthermore, the SHAP values indicate that for most of the features, an increase in feature values leads to an increase in the SHAP values, particularly for features such as mean_3, min_3, SampEn_2, and REn_2, which exhibit more pronounced effects. This provides a clearer understanding of the relationship between feature changes and the model's output, enhancing the explainability of the depression classification process.

F. Internal State Transition of Brain Activity in Depression

The number of states of the TDE-HMM model is a hyperparameter that needs to be determined before the model is trained. After several experiments, we find that 7 hidden states can fully describe the brain activity process under different audio stimulation.

		Computation Time (s)					
Method	Computational Complexity	k-NN	SVM	NB	DT	RF	XGBoost
LASSO	$O(m^2n^2)$	0.08	0.14	0.03	0.16	0.39	0.48
SVM-RFE	$O(m^2 * max(m, n))$	0.18	0.27	0.14	0.31	0.54	0.60
RF	O(mn * log(n))	0.56	0.61	0.50	0.65	0.92	1.06
Fisher	O(mn)	0.07	0.16	0.02	0.19	0.41	0.48
CFS	$O(m^2n)$	0.07	0.16	0.03	0.19	0.43	0.50
InfoGain	O(mn)	0.12	0.21	0.08	0.23	0.41	0.56
ReliefF	$O(mn^2)$	0.99	1.12	0.94	1.14	1.31	1.52
IFS	$O(m^3(1+n)+n^2)$	0.13	0.23	0.09	0.28	0.51	0.76
SCEFS	$O(m^2)$	0.07	0.16	0.02	0.15	0.42	0.49
SCRFS	$O(m^2)$	0.06	0.19	0.02	0.13	0.37	0.78
SCAFS	$O(m^2)$	0.08	0.17	0.05	0.17	0.40	0.57
ALO-MARL	O(fmn * log(n))	95.57	104.57	33.17	162.45	334.46	576.23
ALO	O(mn*log(n))	63.56	77.65	34.69	69.09	126.33	291.27
MARL	O(fmn*log(n))	96.89	94.65	19.76	188.86	414.37	690.07
GA	O(mn*log(n))	121.99	251.58	16.00	258.90	605.92	968.68

TABLE IX

COMPUTATIONAL COMPLEXITY AND TIME OF DIFFERENT FEATURES SELECTION METHODS

^{*} m is the number of features; f is the number of selected features; n is the number of samples.

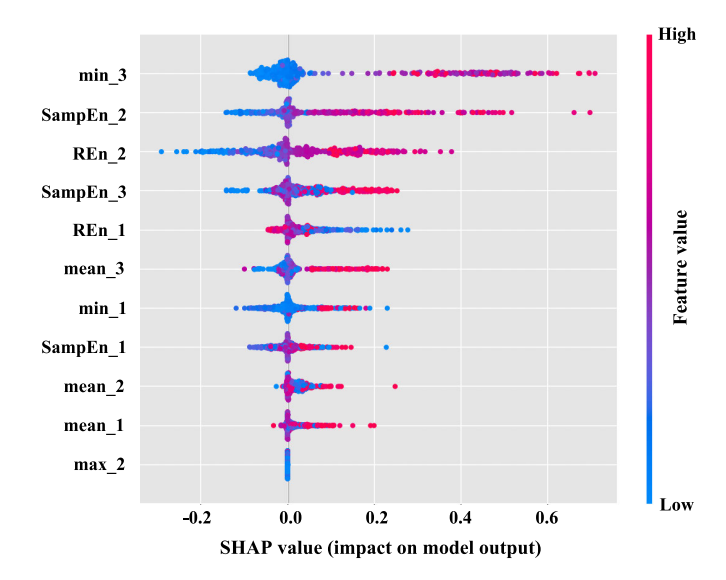


Fig. 4. SHAP summary plot. The ranking of feature importance is displayed. We can see that the most important factor for depression detection according to the model is the indicator of the minimum values of PSD.

Next, we analyses the internal state transition under various audio stimulation by using the TDE-HMM model. Fig. 5 shows the average probability series of 7 HMM states in 12 time phases (As mentioned above, the 12 time phases are alternated between a 6-second resting state and a 6-second audio stimulation state, as shown in Fig. 1). At the beginning, states 4, 5, and 6 have the highest occurrence probability, while states 1, 2, 3, and 7 have the lowest probability. As the audio stimulation proceeds, the probability of state 4, 5, and 6 decreases, and the probability of state 2, 3, and 7 increases as the resting state changes to the stimulated state. During phases 1-4 (neutrally-valenced audio stimulation), state 3 has

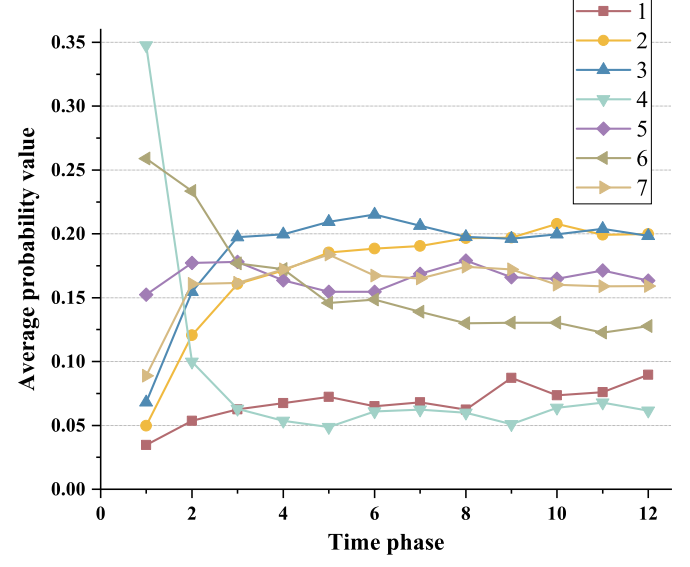


Fig. 5. Establishment of the TDE-HMM model. Average probability values over time of internal states activation. Each state corresponds to a probability series. The amplitude of the probability series represents the probability of the state activation, and the time series is consistent with the sampling frequency of the EEG. The sum of the probabilities of all states at each time point is 1.

the highest probability of occurrence, and states 2, 5, 6, and 7 have similar probabilities. In phases 5-8 (negatively audio stimulation), state 3 continues to increase, and in the last phase, state 2 is equal to state 3, while states 7 and 5 fluctuate. During phases 9-12 (positively-valenced audio stimulation), state 2 has surpassed state 3 and becomes the most frequent state, while states 7 and 5 converge, state 6 continues to decrease, state 1 tends to rise, indicating an enhanced regulatory effect, accelerating the internal state transition, and state 4 appears least frequently.

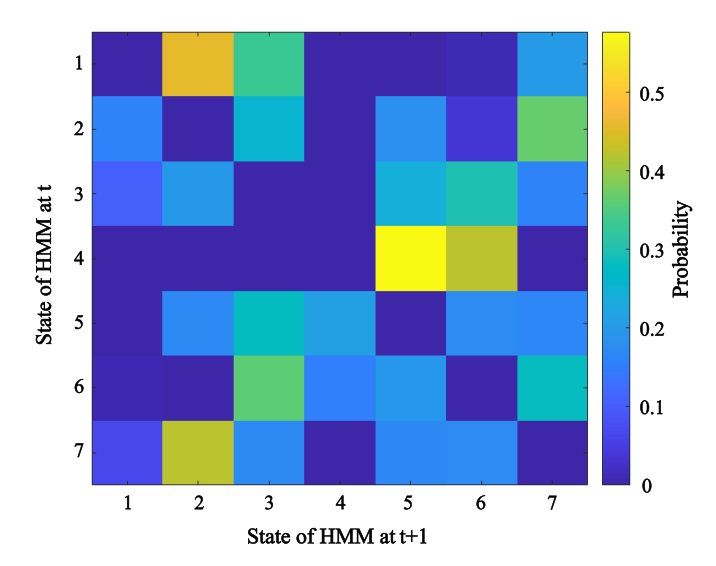


Fig. 6. The state transition probability matrix. The horizontal and vertical axes of the matrix represent the label of the state. The value of each pixel represents the transition probability between states.

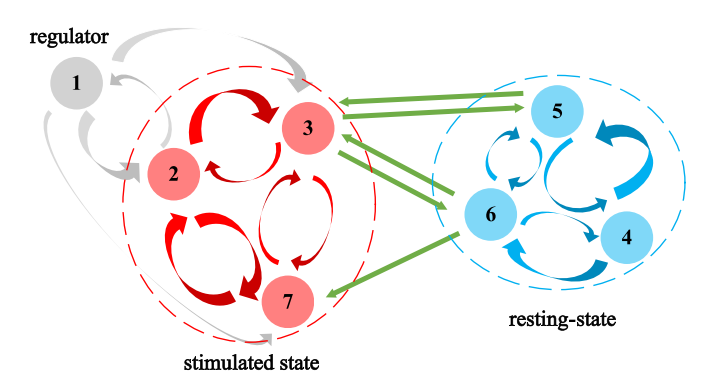


Fig. 7. The topological graph of the state transition. The thicker the line, the stronger the transition probability. The blue circle represents the resting-state, the red circle represents the set of stimulated states, and the number 1 marked in gray indicates the regulator that regulates the transition between stimulated states.

Furthermore, the state transition probability matrix presented in Fig. 6 reveals that there is a considerable probability of transition within the states in different stimulation phases and the resting-state phase. Interestingly, state 1 can be used as a moderator to smooth the transition to different audio stimulation phases. These results are consistent with the above analysis. Based on the state transition probability matrix, the topological graph is obtained, as shown in Fig. 7.

IV. DISCUSSION

A. Depression Recognition Models

In this work, we propose a feature selection model for depression detection based on the ALO-MARL algorithm. To ensure the robustness of the ALO-MARL algorithm, we mix data from 70 depressed patients and 108 healthy controls for training and testing. We have carried out experiments in several aspects.

1) Comparison of Different Feature Selection Algorithms: The study evaluates different classifiers using three feature fusion strategies and four evaluation metrics. As shown in Tables I-VI, the XGBoost classifier performs the best, while the NB classifier performs the worst due to feature elimination in the ALO-MARL algorithm. Furthermore, the proposed ALO-MARL feature fusion method consistently outperforms other methods in terms of recognition effectiveness for most classifiers, except for some cases where specificity remains comparable.

The ALO-MARL algorithm shows considerable improvement in the effectiveness of the SVM classifier, with notable enhancements in sensitivity and F1-score metrics compared to the ALO and MARL algorithms. For instance, this algorithm exhibits a notable enhancement of 15.10% in sensitivity metrics compared to the ALO algorithm, and respective improvements of 13.55% and 26.71% in F1-score and sensitivity metrics compared to the MARL algorithm. Additionally, the algorithm demonstrates superior learning capabilities with smaller feature subsets, as indicated in Table VII.

2) Comparison of Previous State-of-the-Art Models: We present a comprehensive review of previous studies employing prefrontal-lobe three-lead EEG data for depression recognition. Reference [15], [34], and [62] have attained classification accuracies of 83.07%, 86.98%, and 79.27%, respectively. Notably, our innovative approach, developed through the integration of the ALO-MARL algorithm and the XGBoost classifier, demonstrates a commendable classification accuracy of 93.69%.

The identical auditory stimuli EEG dataset employed in [3] is utilized in this investigation. In [3], the ALO algorithm is applied for both feature selection and weighting, in conjunction with a *k*-NN classifier for depression recognition. The resulting metrics, including F1-score, accuracy, sensitivity, and specificity, are reported as 87.33%, 90.70%, 81.79%, and 96.53%, respectively. In contrast, our study employs the ALO-MARL algorithm for feature selection, followed by XGBoost for depression recognition. Notably, the achieved F1-score, accuracy, sensitivity, and specificity in our model are considerably elevated, reaching 91.82% 93.69%, 88.60%, and 97.08%, respectively. This performance surpasses the efficacy demonstrated by the proposed methodology in [3].

In the field of medical diagnostics, the effectiveness of a test relies on striking a delicate balance between sensitivity and specificity. Our innovative approach demonstrates outstanding performance, achieving an accuracy of 93.69%, an elevated F1-score of 91.82%, a high sensitivity of 88.60%, and an enhanced specificity of 97.08%. These results highlight the significant potential of our method in advancing the diagnosis of depression.

3) Discussion on Cross Validation: While cross-validation is widely used to evaluate classification performance, it may still lead to overestimation of performance metrics, such as accuracy and F1 score, due to the potential for information leakage between training and testing sets. To address this issue, nested cross-validation is considered a more robust method [63], as it evaluates the model's performance by incorporating an additional layer of cross-validation for model selection. However, nested cross-validation is computationally expensive, especially for large datasets, and is often impractical for complex algorithms like the ALO-MARL approach used in this study.

In this work, we employed standard cross-validation, which has been shown to yield reliable estimates of model performance under certain conditions, such as when the dataset size is sufficient and the model is well-regularized. Although this method may still lead to slight overestimation of performance metrics, it remains a widely accepted practice in machine learning.

For future research, we recommend considering nested cross-validation to further enhance the reliability of performance evaluation. Additionally, other methods like repeated random splits or stratified sampling could be explored to mitigate potential biases in performance estimation.

4) Computational Complexity: This study employs ALO-MARL as the feature selection algorithm due to its significant advantages as a wrapper-based method. By iteratively evaluating the performance of feature subsets, ALO-MARL effectively captures complex relationships between features, thereby enhancing the overall performance of the model. Although ALO-MARL involves higher computational costs in terms of model construction and runtime compared to embedded or filter-based methods, its notable improvements in performance metrics validate its suitability and superiority for feature selection tasks.

At the same time, to address the issue of feature dimensionality, this study employs a portable three-lead EEG acquisition device for EEG signal analysis. Currently, most commercial portable EEG devices support data acquisition for up to 8 or 16 channels. For data from large-scale EEG channel devices, the proposed ALO-MARL algorithm exhibits a linear increase in computational complexity as the number of features grows, and this complexity is also related to the number of selected features specified by the algorithm. Compared to other feature selection methods, although all methods experience some degree of reduction in computational efficiency, the experimental results show that the ALO-MARL algorithm outperforms others in terms of performance metrics.

When using RL to address feature selection, the need for training and prediction at each step results in substantial computational overhead. However, with sufficient computational resources, such as GPUs or parallel computing, this high computational demand may not pose a significant bottleneck. For instance, in many scenarios, the model optimization process can be conducted offline, and the optimized feature subset can subsequently be used for rapid prediction in real-time applications, striking a balance between computational cost and operational efficiency.

For applications with low real-time requirements, such as medical diagnostics or other offline analysis tasks, longer training times are acceptable. In such cases, even though the computational efficiency may be lower, the substantial improvements in model performance justify the adoption of this method.

B. XAI for Model Post Interpretation Results

The classification model undergoes post-interpretation employing two XAI methodologies. The results, as depicted in Fig. 3 and Fig. 4, reveal a congruence in the interpretative outcomes derived from both methods. Notably, the minimal

value of PSD, SampEn, and REn collectively exert the most pronounced influence on the model.

The observation underscores the critical importance of these three factors in the context of depression recognition, positing them as indispensable contributors that demand careful consideration. Omitting any of these factors may compromise the accuracy and efficacy of the model.

C. Internal State Transition Within the Brain

Numerous scholarly articles currently address issues related to state transitions in EEG studies. In [64], the authors aim to elucidate the spatiotemporal complexity of whole-brain networks and state transitions during sleep. Their results unveil critical trajectories governing transitions within and between sleep stages based on EEG data. Reference [65] reveals substantial alterations in brain activity and connectivity during epileptic seizures, as the brain network transitions from a balanced resting state to a hyperactive and hypersynchronous state. In [48], an experiment is designed to validate the impact of acupuncture stimulation on the human brain. Experimental results indicate that acupuncture can activate novel brain states, with different acupuncture techniques inducing state transitions along independent pathways. The focus of this present study lies in examining the state changes in EEG patterns of individuals with depression under various auditory stimuli.

Many conclusions can be drawn from the previous analyses, especially through the topological graph as well as the state transition probability matrix. It can be found that except for state 1, the other states are activated periodically, which is closely related to the phases of time. In particular, states 4, 5, and 6 are mainly activated during the resting-state, while the states 2, 3, and 7 are closely related to different audio stimulation. The states of different audio stimulation are all within one set. The study shows that the internal state transition in the brain of depressed patients appears flexible and that these states seem activated alternating over time. Furthermore, such transitions appear not only induced within the overall state of the audio stimulation, but appear also activated between the resting state and the stimulation phase.

The most obvious finding from Fig. 7 is that there is a direct state transition pathway between the resting-state and the stimulated states. Furthermore, there are differences in the transition pathways between resting and stimulated states. For example, there are multiple transition pathways (states 5-3, states 6-3, and states 6-7) from the resting-state phase to the stimulation phase, but only 2 transition pathways (states 3-5 and states 3-6) from the stimulation phase to the resting-state phase. So far, these findings suggest that audio stimulation can modulate brain states in patients with depressive disorders and that different audio stimulation can induce state transitions in a hybrid pathway.

D. Analysis of the Advantages and Innovations of the ALO-MARL Algorithm

Although the ALO-MARL algorithm has a disadvantage in terms of computational complexity, specifically longer

training time, it offers several advantages in feature selection, as detailed below.

- 1) Accuracy Improvement: The primary advantage of ALO-MARL lies in its enhanced classification accuracy, achieving 93.69% compared to approximately 90% with traditional feature selection methods like Fisher, SVM-RFE, and CFS. Although the training and prediction time is longer, the increased accuracy is significant, especially for high-stakes applications such as medical diagnostics, where even a small improvement in accuracy can result in substantially better outcomes.
- 2) Suitability for Complex Datasets: ALO-MARL is particularly effective with high-dimensional datasets, such as EEG data with numerous variables and channels. Traditional methods like Fisher, SVM-RFE, and CFS may face performance limitations as feature dimensionality increases. In contrast, ALO-MARL's MARL component enables effective feature fusion and selection, allowing for better feature representation and generalization on complex datasets.
- 3) Quality of Feature Selection: ALO-MARL's combination of optimization and feature fusion results in selected features that not only enhance classification performance but may also exhibit greater interpretability and stability. This aspect is crucial in medical domains, where selected features should ideally reflect meaningful neurophysiological insights rather than being purely optimized for mathematical purposes.
- 4) Long-Term Cost Trade-off: Although ALO-MARL has a longer training time, the model can be deployed for fast predictions once training is complete, making the increased training time acceptable in scenarios involving one-time optimization or offline analysis. Additionally, as computational resources and hardware continue to improve, ALO-MARL's computation time can be reduced without compromising its high accuracy in complex feature selection tasks.
- 5) Novelty and Research Value: The ALO-MARL algorithm offers a novel approach to feature selection, integrating MARL in a way that is relatively rare in current feature selection methodologies. Its innovation adds significant research value and can be further substantiated by a detailed comparison with traditional methods to illustrate its scope and advantages.

Through a detailed analysis of these aspects, it is possible to argue that, although the computational cost of ALO-MARL is higher, its advantages in terms of selection accuracy, suitability for high-dimensional data, feature selection quality, and novelty make it a highly competitive approach for EEG data processing tasks.

E. Limitations and Future Work

This work still faces some limitations. The proposed ALO-MARL algorithm, as a wrapper-based feature selection method, has a higher computational complexity compared to other embedded and filter-based feature selection methods. However, its computational complexity is moderate when compared to other wrapper-based methods, remaining within a reasonable range. Despite this, the outstanding performance of the ALO-MARL algorithm can somewhat compensate for the drawbacks associated with its computational complexity.

Future work will focus on optimizing the computational complexity of the algorithm. In terms of model development, efforts will be made to achieve model lightweighting, such as through pruning and distillation techniques, while maintaining the performance advantages of the model. When using RL to solve feature selection tasks, the need for training and prediction at each step can significantly increase computational costs. To address this, future work will explore strategies to reduce computational demands, such as using lighter proxy models to approximate performance evaluation during the RL process (e.g., simple models based on prior knowledge). Additionally, the training time can be reduced in intermediate steps of feature selection optimization, with the main model being used only in the final evaluation phase. If resources permit, the training process may also be distributed across multiple devices or nodes to execute in parallel, aiming to significantly accelerate the feature selection optimization process. Although using RL for feature selection presents challenges in computational efficiency, it is hoped that these challenges can be mitigated through appropriate optimization strategies, particularly in offline analysis or when distributed computing is feasible. Future work will also focus on the analysis of low-dimensional manifold dynamics of the human brain. Low-dimensional dynamics and neural manifolds can help understand the temporal dynamics and dynamic changes of the human brain during audio stimulation, providing a new perspective for further improving the clinical application of music therapy for depression.

V. CONCLUSION

This paper provides a post-interpretation of a classification model to clarify which features have a stronger impact on the classification task and to reveal important factors affecting depression detection. We implemented EEG feature selection using the ALO-MARL algorithm, ultimately identifying features highly relevant to the depression recognition task. The depression recognition accuracy achieved was 93.69%. Further research was conducted on the internal state transition of the brain in patients with depression under audio stimulation to reveal the modulation effect of external stimulation and further explain the results of depression recognition. Post interpretation of depression recognition results using XAI methods showed that the PSD and SampEn are strongly correlated with depression recognition. This study enhances the explainability of the depression recognition task. Furthermore, the internal states of the brain in depression during audio stimulation were inferred with a TDE-HMM. It was observed that the brain activity was best modelled as transitioning within an ensemble of states and that audio stimulation appears to be able to evoke new brain states. The obtained results could give an insight into how audio stimulation can improve the brain cognition by regulating internal state transition, and explain the results of depression recognition to further reveal the mechanism of depression activation.

For clinicians, this type of neural feature information may provide valuable insights to uncover additional associations related to depression. For neuroscientists, it offers a deeper understanding of the pathophysiological mechanisms underlying depression. For fellow researchers, the introduction of MARL presents a novel and more effective approach to EEG feature selection.

REFERENCES

- [1] H. Cai, "A multi-modal open dataset for mental-disorder analysis," *Sci. Data*, vol. 9, no. 1, p. 178, Apr. 2022.
- [2] Depression and Other Common Mental Disorders: Global Health Estimates, World Health Org. (WHO), Geneva, Switzerland, 2017.
- [3] F. Tian et al., "The three-lead EEG sensor: Introducing an EEG-assisted depression diagnosis system based on ant lion optimization," *IEEE Trans. Biomed. Circuits Syst.*, vol. 17, no. 6, pp. 1305–1318, Jun. 2023.
- [4] L. Chennapragada et al., "International PRISMA scoping review to understand mental health interventions for depression in COVID-19 patients," *Psychiatry Res.*, vol. 316, Oct. 2022, Art. no. 114748.
- [5] J. B. Frøkjær et al., "Integrity of central nervous function in diabetes mellitus assessed by resting state EEG frequency analysis and source localization," *J. Diabetes Complications*, vol. 31, no. 2, pp. 400–406, Feb. 2017.
- [6] X. Li, B. Hu, T. Xu, J. Shen, and M. Ratcliffe, "A study on EEG-based brain electrical source of mild depressed subjects," *Comput. Methods Programs Biomed.*, vol. 120, no. 3, pp. 135–141, Jul. 2015.
- [7] H. Cai, X. Zhang, Y. Zhang, Z. Wang, and B. Hu, "A case-based reasoning model for depression based on three-electrode EEG data," *IEEE Trans. Affect. Comput.*, vol. 11, no. 3, pp. 383–392, Jul. 2020.
- [8] B. Wang, Y. Kang, D. Huo, D. Chen, W. Song, and F. Zhang, "Depression signal correlation identification from different EEG channels based on CNN feature extraction," *Psychiatry Res.*, *Neuroimaging*, vol. 328, Jan. 2023, Art. no. 111582.
- [9] B. Hu, L. Zhu, Q. Dong, K. Qian, H. Cai, and F. Tian, "Physiological electrosignal asynchronous acquisition technology: Insight and perspectives," *IEEE Trans. Computat. Social Syst.*, vol. 11, no. 1, pp. 5–24, Feb. 2024.
- [10] L. Shen et al., "A first look at generative artificial intelligence based music therapy for mental disorders," *IEEE Trans. Consum. Electron.*, early access, Dec. 9, 2024, doi: 10.1109/TCE.2024.3514633.
- [11] L. Zhu et al., "Design and implementation of electroacupuncture: A study of prefrontal EEG characteristics under taVNS," *IEEE Sensors J.*, vol. 24, no. 20, pp. 32533–32545, Oct. 2024.
- [12] F. Tian et al., "An on-board executable multi-feature transfer-enhanced fusion model for three-lead EEG sensor-assisted depression diagnosis," *IEEE J. Biomed. Health Informat.*, vol. 29, no. 1, pp. 152–165, Jan. 2025.
- [13] G. Chandrashekar and F. Sahin, "A survey on feature selection methods," Comput. Elect. Eng., vol. 40, no. 1, pp. 16–28, Jan. 2014.
- [14] W. Tu and S. Sun, "Spatial filter selection with LASSO for EEG classification," in *Proc. 6th Int. Conf. Adv. Data Mining Appl.*, Berlin, Germany. Cham, Switzerland: Springer, Jan. 2010, pp. 142–149.
- [15] H. Cai, Z. Qu, Z. Li, Y. Zhang, X. Hu, and B. Hu, "Feature-level fusion approaches based on multimodal EEG data for depression recognition," *Inf. Fusion*, vol. 59, pp. 127–138, Jul. 2020.
- [16] F. Hassan, S. F. Hussain, and S. M. Qaisar, "Fusion of multivariate EEG signals for schizophrenia detection using CNN and machine learning techniques," *Inf. Fusion*, vol. 92, pp. 466–478, Apr. 2023.
- [17] A. Holzinger, G. Langs, H. Denk, K. Zatloukal, and H. Müller, "Causability and explainability of artificial intelligence in medicine," WIRES Data Mining Knowl. Discovery, vol. 9, no. 4, p. 1312, Jul. 2019.
- [18] L. Breiman, "Random forests," Mach. Learn., vol. 45, pp. 5–32, Oct. 2001.
- [19] S. M. Lundberg and S.-I. Lee, "A unified approach to interpreting model predictions," in *Proc. 31st Int. Conf. Neural Inf. Process. Syst.*, 2017, pp. 4768–4777.
- [20] M. Gandolfi et al., "Explainable AI allows predicting upper limb rehabilitation outcomes in sub-acute stroke patients," *IEEE J. Biomed. Health Informat.*, vol. 27, no. 1, pp. 263–273, Jan. 2023.
- [21] F. Tian et al., "An FFT-based DC offset compensation and I/Q imbalance correction algorithm for bioradar sensors," *IEEE Trans. Microw. Theory Techn.*, vol. 72, no. 3, pp. 1900–1910, Mar. 2024.
- [22] R. W. Homan, J. Herman, and P. Purdy, "Cerebral location of international 10–20 system electrode placement," *Electroencephalogr. Clin. Neurophysiology*, vol. 66, no. 4, pp. 376–382, Apr. 1987.

- [23] M. M. Bradley and P. J. Lang, The International Affective Digitized Sounds (IADS-2): Affective Ratings of Sounds and Instruction Manual. Gainesville, FL, USA: Univ. of Florida Press, 2007.
- [24] Q. Shi et al., "High-speed ocular artifacts removal of multichannel EEG based on improved moment matching," J. Neural Eng., vol. 18, no. 5, Oct. 2021, Art. no. 056038.
- [25] C. J. Stam, "Nonlinear dynamical analysis of EEG and MEG: Review of an emerging field," *Clin. Neurophysiol.*, vol. 116, no. 10, pp. 2266–2301, Oct. 2005.
- [26] V. A. Grin-Yatsenko, I. Baas, V. A. Ponomarev, and J. D. Kropotov, "EEG power spectra at early stages of depressive disorders," *J. Clin. Neurophysiology*, vol. 26, no. 6, pp. 401–406, 2009.
- [27] D. J. A. Smit, D. Posthuma, D. I. Boomsma, and E. J. C. De Geus, "The relation between frontal EEG asymmetry and the risk for anxiety and depression," *Biol. Psychol.*, vol. 74, no. 1, pp. 26–33, Jan. 2007.
- [28] D. Mathersul, L. M. Williams, P. J. Hopkinson, and A. H. Kemp, "Investigating models of affect: Relationships among EEG alpha asymmetry, depression, and anxiety," *Emotion*, vol. 8, no. 4, pp. 560–572, 2008
- [29] E. Jesulola, C. F. Sharpley, V. Bitsika, L. L. Agnew, and P. Wilson, "Frontal alpha asymmetry as a pathway to behavioural withdrawal in depression: Research findings and issues," *Behavioural Brain Res.*, vol. 292, pp. 56–67, Oct. 2015.
- [30] M. Aboy, R. Hornero, D. Abasolo, and D. Alvarez, "Interpretation of the lempel-ziv complexity measure in the context of biomedical signal analysis," *IEEE Trans. Biomed. Eng.*, vol. 53, no. 11, pp. 2282–2288, Nov. 2006.
- [31] L. Zhao, L. Yang, B. Li, Z. Su, and C. Liu, "Frontal alpha complexity of different severity depression patients," *J. Healthcare Eng.*, vol. 2020, pp. 1–8, Sep. 2020.
- [32] J. S. Richman and J. R. Moorman, "Physiological time-series analysis using approximate entropy and sample entropy," Amer. J. Physiol.-Heart Circulatory Physiol., vol. 278, no. 6, pp. H2039–H2049, Jun. 2000.
- [33] A. Rényi, "On measures of entropy and information," in *Proc. 4th Berkeley Symp. Math. Statist. Probab., Contrib. Theory Statist.*, vol. 4. Berkeley, CA, USA: Univ. California Press, 1961, pp. 547–562.
- [34] J. Shen, S. Zhao, Y. Yao, Y. Wang, and L. Feng, "A novel depression detection method based on pervasive EEG and EEG splitting criterion," in *Proc. IEEE Int. Conf. Bioinf. Biomed. (BIBM)*, Nov. 2017, pp. 1879–1886.
- [35] A. C. Cinar, "A novel adaptive memetic binary optimization algorithm for feature selection," *Artif. Intell. Rev.*, vol. 56, no. 11, pp. 13463– 13520, Nov. 2023.
- [36] I. Niño-Adan, D. Manjarres, I. Landa-Torres, and E. Portillo, "Feature weighting methods: A review," *Expert Syst. Appl.*, vol. 184, Dec. 2021, Art. no. 115424.
- [37] L. Abualigah, M. Shehab, M. Alshinwan, S. Mirjalili, and M. A. Elaziz, "Ant lion optimizer: A comprehensive survey of its variants and applications," *Arch. Comput. Methods Eng.*, vol. 28, no. 3, pp. 1397–1416, May 2021.
- [38] S. Gronauer and K. Diepold, "Multi-agent deep reinforcement learning: A survey," *Artif. Intell. Rev.*, vol. 55, no. 2, pp. 895–943, 2022.
- [39] S. Mirjalili, "The ant lion optimizer," Adv. Eng. Softw., vol. 83, pp. 80–98, May 2015.
- [40] D. Singh and B. Singh, "Hybridization of feature selection and feature weighting for high dimensional data," *Int. J. Speech Technol.*, vol. 49, no. 4, pp. 1580–1596, Apr. 2019.
- [41] X. Li, X. Hu, R. Zhang, and L. Yang, "Routing protocol design for underwater optical wireless sensor networks: A multiagent reinforcement learning approach," *IEEE Internet Things J.*, vol. 7, no. 10, pp. 9805–9818, Oct. 2020.
- [42] K. Malialis, J. Wang, G. Brooks, and G. Frangou, "Feature selection as a multiagent coordination problem," 2016, arXiv:1603.05152.
- [43] C. Holmesparker, M. E. Taylor, A. K. Agogino, and K. Tumer, "CLEAN rewards to improve coordination by removing exploratory action noise," in *Proc. IEEE/WIC/ACM Int. Joint Conf. Web Intell. (WI) Intell. Agent Technol. (IAT)*, vol. 3, Aug. 2014, pp. 127–134.
- [44] A. Altmann, L. Toloşi, O. Sander, and T. Lengauer, "Permutation importance: A corrected feature importance measure," in *Proc. Bioinf.*, Apr. 2010, vol. 26, no. 10, pp. 1340–1347.
- [45] L. S. Shapley, "A value for n-person games," in *Contributions to the Theory of Games*, vol. 2, H. W. Kuhn and A. W. Tucker, Eds., Princeton, NJ, USA: Princeton Univ. Press, 1953, pp. 307–318, doi: 10.1515/9781400881970-018.

- [46] M. L. Baptista, K. Goebel, and E. M. P. Henriques, "Relation between prognostics predictor evaluation metrics and local interpretability SHAP values," *Artif. Intell.*, vol. 306, May 2022, Art. no. 103667.
- [47] J. K. Grewal, "Markov models-hidden Markov models," *Nature Methods*, vol. 16, pp. 795–796, Mar. 2019.
- [48] H. Yu, D. Liu, S. Li, J. Wang, J. Liu, and C. Liu, "Probing the flexible internal state transition and low-dimensional manifold dynamics of human brain with acupuncture," *Biomed. Signal Process. Control*, vol. 82, Apr. 2023, Art. no. 104494.
- [49] S. Zhang, X. Li, M. Zong, X. Zhu, and R. Wang, "Efficient kNN classification with different numbers of nearest neighbors," *IEEE Trans. Neural Netw. Learn. Syst.*, vol. 29, no. 5, pp. 1774–1785, May 2018.
- [50] H. Zhang, "The optimality of naive Bayes," in Proc. 17th Int. Florida Artif. Intell. Res. Soc. Conf. (FLAIRS), 2004, vol. 1, no. 2, p. 3.
- [51] H. Zhou, J. Zhang, Y. Zhou, X. Guo, and Y. Ma, "A feature selection algorithm of decision tree based on feature weight," *Expert Syst. Appl.*, vol. 164, Feb. 2021, Art. no. 113842.
- [52] J. Sun, H. Yu, G. Zhong, J. Dong, S. Zhang, and H. Yu, "Random Shapley forests: Cooperative game-based random forests with consistency," *IEEE Trans. Cybern.*, vol. 52, no. 1, pp. 205–214, Jan. 2022.
- [53] T. Chen and C. Guestrin, "XGBoost: A scalable tree boosting system," in *Proc. 22nd ACM SIGKDD Int. Conf. Knowl. Discovery Data Mining*, Aug. 2016, pp. 785–794.
- [54] X. Li, B. Hu, S. Sun, and H. Cai, "EEG-based mild depressive detection using feature selection methods and classifiers," *Comput. Methods Programs Biomed.*, vol. 136, pp. 151–161, Nov. 2016.
- [55] G. Roffo et al., "Infinite feature selection: A graph-based feature filtering approach," *IEEE Trans. Pattern Anal. Mach. Intell.*, vol. 43, no. 12, pp. 4396–4410, Jun. 2021.

- [56] J. Zhang, M. Chen, S. Zhao, S. Hu, Z. Shi, and Y. Cao, "Relieff-based EEG sensor selection methods for emotion recognition," *Sensors*, vol. 16, no. 10, p. 1558, Sep. 2016.
- [57] Q. Gu, Z. Li, and J. Han, "Generalized Fisher score for feature selection," in *Proc. 27th Conf. Uncertainty Artif. Intell.* Arlington, VA, USA: AUAI Press, Jul. 2011, pp. 266–273.
- [58] B. Azhagusundari, A. S. Thanamani, and D. A. S. Thanamani, "Feature selection based on information gain," in *Proc. Comput. Sci., Math.*, 2013, pp. 1–12.
- [59] I. Guyon, J. Weston, S. Barnhill, and V. Vapnik, "Gene selection for cancer classification using support vector machines," *Mach. Learn.*, vol. 46, no. 1, pp. 389–422, 2002.
- [60] A. Saibene and F. Gasparini, "Genetic algorithm for feature selection of EEG heterogeneous data," Expert Syst. Appl., vol. 217, May 2023, Art. no. 119488.
- [61] J. Xie, M. Wang, S. Xu, Z. Huang, and P. W. Grant, "The unsupervised feature selection algorithms based on standard deviation and cosine similarity for genomic data analysis," *Frontiers Genet.*, vol. 12, 2021, Art. no. 684100.
- [62] H. Cai et al., "A pervasive approach to EEG-based depression detection," Complexity, vol. 2018, pp. 1–13, Jan. 2018.
- [63] G. Varoquaux, P. R. Raamana, D. A. Engemann, A. Hoyos-Idrobo, Y. Schwartz, and B. Thirion, "Assessing and tuning brain decoders: Cross-validation, caveats, and guidelines," *NeuroImage*, vol. 145, pp. 166–179, Jan. 2017.
- [64] A. B. A. Stevner et al., "Discovery of key whole-brain transitions and dynamics during human wakefulness and non-REM sleep," *Nature Commun.*, vol. 10, no. 1, p. 1035, Mar. 2019.
- [65] C. D. Verdugo et al., "Glia-neuron interactions underlie state transitions to generalized seizures," *Nature Commun.*, vol. 10, no. 1, p. 3830, Aug. 2019.